Eur Biophys J (2009) 38:971–980
DOI 10.1007/s00249-009-0488-z

ORIGINAL PAPER

Early detection of premalignant changes in cell cultures using light-induced fluorescence spectroscopy

E. Bogomolny · Shaul Mordechai · A. Zwielly · M. Huleihel

Received: 18 February 2009 / Revised: 7 May 2009 / Accepted: 13 May 2009 / Published online: 5 June 2009

Abstract Light-induced fluorescence (LIF) spectroscopy has demonstrated ability as a novel, noninvasive and sensitive technology for early detection of cancer. The goal of the present study is to examine the potential of this spectroscopic method for early detection and characterization of premalignant changes. As a model we used both cell lines and primary cells, which were transformed to malignant by retrovirus. Fluorescence measurements and morphological observations of the infected cells were performed at various postinfection times. Our results showed gradual attenuation of fluorescence intensities due to cancer progression which corresponds to aromatic amino acids and nicotinamide adenine dinucleotide (NADH) molecules. In order to obtain grading and supervised classifications of the spectral premalignant changes we used approaches of linear discriminant analysis. The classifications based on Mahalanobis distances allowed us to demonstrate that the accuracy of identification of premalignant stages varied between 83.1% and 96.4%. In summary, we conclude that LIF in tandem with proper statistical tools may be a promising technique for early detection of malignant progression.

E. Bogomolny · S. Mordechai (✉) · A. Zwielly
Department of Physics, Ben Gurion University,
84105 Beersheba, Israel
e-mail: shaulm@bgu.ac.il

M. Huleihel (✉)
Department of Virology and Developmental Genetics,
Medical School, Ben-Gurion University of the Negev,
84105 Beersheba, Israel
e-mail: mahmoudh@bgu.ac.il

Keywords Light-induced fluorescence · Malignant transformation · Linear discriminant analysis · Discriminant classification function · Early diagnosis

Introduction

In recent years, ultraviolet and infrared spectroscopy have been studied for the development of novel, noninvasive and sensitive, real-time technologies that can identify malignancy in situ. Among these spectroscopic techniques, special interest has been aroused by methods based on endogenous fluorescence due to their potential as an unsophisticated reagent-free technology (Bigio and Mourant 1997; Mayinger et al. 2001). The principal advantage of fluorescence over absorption spectroscopy is the ability to separate compounds based on either their excitation or emission spectra. Moreover, only molecules with significant quantum yield are detectable, thus biological interpretation and quantitative estimation is much easier compared with highly overlapping infrared (IR) spectra.

Previous studies applying different fluorescence approaches succeeded in distinguishing between normal and malignant cells in various types of tissues. These works include breast (Breslin et al. 2004; Alfano et al. 1991), colorectal (Horak et al. 2006), cervical (Chidananda et al. 2006; Krishna et al. 2008), oral (Ebihara et al. 2003), and skin cancer (Brancaleon et al. 2007), and also cell lines model (Grossman et al. 2001). There are also studies which address premalignant diagnosis (Sokolov et al. 2002; Zheng et al. 2004; Alvarez et al. 2007; Chaudhury et al. 2001; Georgakoudi et al. 2002; Wang et al. 1999; Kamath and Mahato 2007; Svanberg et al. 1998). Despite achievements in certain areas, the potential of fluorescence spectroscopy still remains relatively unexplored; for

example, the studies mentioned above concentrated on discrimination of visible carcinogenesis changes (for instance, mild dysplasia of cervical cancer [CIN1], defined as dysplastic cells occupying the lower third of the epithelium) without mentioning initiation (where morphological changes can be observed) or continuous monitoring of malignancy.

In many cases, diagnosis of early malignancies in cells/tissues is made by morphological identification. Thus, the detection of malignancy relies heavily on the clinical experience of the examiner in recognizing suspicious lesions during physical examination. Moreover, distinguishing premalignant and early malignant lesions from more common benign inflammatory conditions can be extremely difficult, even for experienced practitioners; for example, cervical Pap smear cytology has an estimated 20–40% false-negative rate, attributed to a combination of inadequate specimen collection, problems inherent to sampling small or inaccessible lesions, and errors in the microscopic reading of the cytology specimen (Solomon 2003). The development of a reagent-free method that allows rapid and accurate diagnosis of malignant lesions in real time would have great potential for improving the early detection of neoplastic changes in cells/tissues. In the majority of cases, this would lead to increased survival chances of patients.

The goal of this research was to examine the potential of light-induced fluorescence (LIF) for early detection and characterization of premalignant changes. For this purpose we used murine sarcoma virus, which transforms normal cell cultures to malignant. Cell cultures are advantageous and more convenient for basic research, compared with "real" tissues, due to their homogeneity and the ability to monitor dysplastic changes over a short time span, therefore this in vitro controlled model can provide more consistent and accurate follow-up.

Methodology

Cell cultures and viruses

Murine fibroblast cell lines (NIH/3T3, long-term in vitro) and mouse embryonic fibroblast cells (MEF, primary cells) were grown at 37°C in Roswell Park Memorial Institute (RPMI) medium supplemented with 10% new born calf serum (NBCS) and the antibiotics penicillin, streptomycin, and neomycin. Incubation was carried out in a humidified atmosphere of 5% CO_2 and 95% air, regulated automatically.

Clone 124 of TB cells chronically releasing Moloney murine sarcoma virus (MuSV-124) was used to prepare a virus stock that contained an approximately 30-fold excess of MuSV particles over Moloney murine leukemia virus (MuLV) particles. The stock was used in the present study in order to transform normal cells in culture to malignant cells.

Cell infection and determination of malignant transformation

Monolayers of NIH/3T3 and MEF cells were grown in 9-cm^2 tissue culture plates and treated with 0.8 μg ml^{-1} polybrene (a cationic polymer required for neutralizing the negative charge of the cell membrane) for 24 h before infection with the virus. Free polybrene was then removed. The cells were incubated with the infecting virus stock in RPMI medium containing 2% NBCS at 37°C for 2 h. As a control group, we incubated the cells with medium containing 2% serum without the infecting virus. The unabsorbed virus particles were removed, fresh medium containing 2% NBCS was added, and the monolayers were incubated at 37°C (similar to control group). After various postinfection time intervals, the cell cultures were carefully examined for the appearance of malignant transformed cells by the following methods in parallel:

(a) Morphological observations
(b) Growth on soft agar (Salman et al. 2003)
(c) LIF measurements

Sample preparation for LIF measurements

Cell cultures were picked up from the culture plates after treatment with trypsin (0.25%). The cells were pelleted by centrifugation at 1,000 rpm for 5 min. Each pellet was washed and resuspended twice with physiological saline solution. The number of cells was counted by a hematocytometer and a concentration of 4×10^5 cells ml^{-1} physiological saline solution was adopted as optimal for spectral measurements, because it preserves linear dependence with fluorescence intensity.

Light-induced fluorescence

Spectra were measured by using Varian Cary Eclipse fluorescence spectrophotometer supplied with Czerny-Turner monochromators, Xenon pulse lamp with exceptionally long lifetime, R928 photomultiplier (PM) tubes, and cuvette and microplate accessories for fluorescence measurements.

Monochromators

Both emission and excitation monochromators have f3.6, 0.125 m focal length with the following characteristics of diffraction gratings:

(a) Emission monochromator has 30 × 35 mm, 1,200 l mm^{-1}, and blaze at 370 nm.
(b) Excitation monochromator has 30 × 35 mm, 1,200 l mm^{-1}, blaze at 440 nm.

Xenon lamp

The xenon lamp produces pulses with power equivalent to 75 kW. Width at half-peak height is ~2 μs. Operational wavelength range for excitation and emission is 200–900 nm with standard Photomultiplier tube. It has wavelength accuracy of ±1.5 nm and wavelength reproducibility of ±0.2 nm.

Photomultiplier tubes (PMTs)

PMT detectors used in fluorescence spectrophotometer are R928 type, with wide spectral response from 185 to 900 nm, high cathode and anode sensitivity, extremely high quantum efficiency, and good signal-to-noise (S/N) ratio.

Accessories

(a) A standard quartz cuvette with 1 cm path length and 3.5 ml volume was used to obtain emission and excitation spectra. Each sample was measured at least three times.
(b) A microplate with 96 wells and 0.5 ml volume for each well was used to obtain fluorescence intensities (Fig. 1). The intensities were based on centroids of emission and excitation spectra. Each sample was measured at least five times in 12 wells, i.e., 60 measurements for each sample.

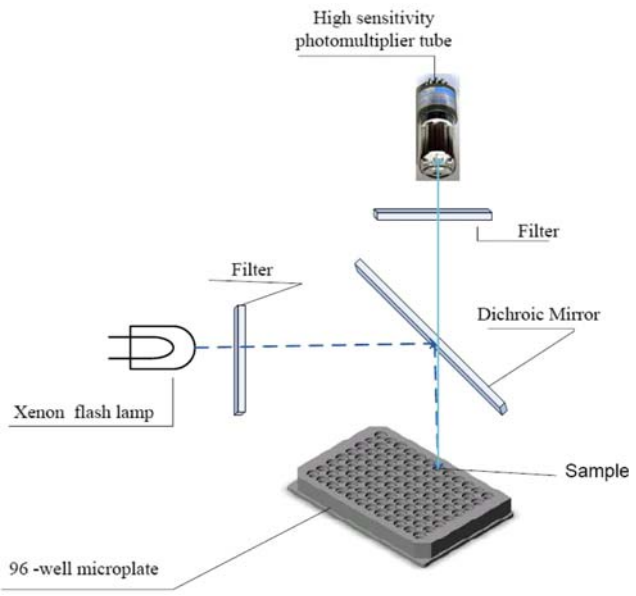

Fig. 1 Schematic plot of the Varian Cary Eclipse microplate reader accessory

Statistical analysis

Linear discriminant analysis (LDA) is a commonly used technique for data classification which maximizes the ratio of the between-class variance to the within-class variance in any particular data set, thereby guaranteeing maximal separability. Two LDA approaches [discriminant classification function (DCF) and Mahalanobis distance] were employed in order to characterize and classify bivariate premalignant change (Fisher 1936; Huberty 1994; Fukunaga 1990). Differences were considered significant at $P < 0.05$.

Results

Determination of fluorescence changes due to malignancy

In order to discern spectral differences between normal (control) and completely transformed cells in culture (NIH/3T3 and MEF), we examined emission and excitation spectra. We focused on spectral regions of endogenous fluorophores with high quantum yield such as aromatic amino acids (tryptophan, tyrosine, phenylalanine) and NADH coenzyme (Lakowicz 1999; Valeur 2002). Figure 2 shows combined average emission spectra of ten samples of normal and completely transformed cell cultures in these two regions (the spectra were cut and baseline-corrected in order to be comparable). Using quartz cuvette we determined that the centroid of aromatic amino acid fluorescence is at 338 nm for NIH/3T3 cell lines with excitation at 285 nm. For MEF primary cells, the fluorescence centroid in same aromatic amino acids region was determined to be at 342 nm at excitation at 285 nm, while fluorescence of NADH coenzyme had centroids at 440 and 433 nm with excitation at 340 nm for these cells in culture. For measuring aromatic amino acids fluorescence the PMT detector was set to medium (600 V), while fluorescence of NADH was measured when PMT voltage was set to high (800 V), since quantum yield is much lower for this intrinsic fluorophore. Our results showed (Fig. 2) that the emission spectra of normal cell cultures were lower than those of the transformed counterparts. However, the fluorescence measurement of quartz cuvette has several disadvantages: (a) it takes a relatively long time interval to scan wavenumber regions, causing variability due to cell residuing, (b) only one sample measurement can be done during this time interval,

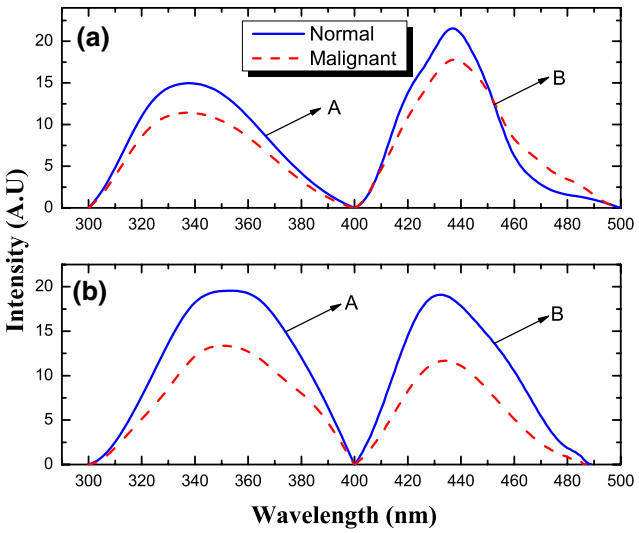

Fig. 2 Combined emission spectra of **a** normal murine fibroblast cell line (NIH/3T3) and completely transformed fibroblast cell line. **b** Combined emission spectra of normal mouse embryonic cells (MEF cells) and completely transformed mouse embryonic cells. The aromatic amino acid fluorescence region, labeled "A", is 300–400 nm due to excitation at 285 nm, with PMT set at 600 V. The NADH fluorescence region, labeled "B", is 400–500 nm due to excitation at 340 nm, with PMT set at 800 V

and (c) it requires a large amount of cells to obtain the concentrations necessary for the cuvette volume. Thus, we used a microplate with 96 wells, which allows detection based on excitation and emission wavelength centroids only. We measured fluorescence of 40 samples of normal and transformed NIH/3T3 cell line and also 28 samples of normal and transformed MEF primary cells (60 repetitions for each sample). In order to examine separability between normal and transformed cells in culture based on the above-discussed fluorophores we assumed that our data had two-dimensional Gaussian distribution with probability distribution density expressed as follows:

$$P(x_1, x_2) = \frac{1}{2\pi\sqrt{|\sum|}}\exp\left(-\frac{1}{2}[X-\mu]^T\Sigma^{-1}[X-\mu]\right) \quad (1)$$

where Σ is the data covariance for each group, expressed as

$$\sum_{ij} = \frac{1}{n}\sum_{n=1}^{n}(X_i-\mu)^T(X_j-\mu), \quad (2)$$

where X_i is bivariate sample, and μ is the mean of the group. Figure 3a, b shows the bivariate model of Gaussian scattering for both cells in culture. As can be seen from Fig. 3 the intensities of normal cells in culture are significantly higher than the malignant cells and both can be statistically separated using the posterior probabilities. Even though the groups are significantly different, it is necessary to examine whether the fluorescence changes come from malignancy. In order to determine whether the viral proteins contributed to the spectral changes observed in the transformed cells or not, we infected cells with MuLV, which is incapable of cell transformation, while it has similar protein structure to MuSV. The results showed that the values of the above biomarkers were identical to the control uninfected cells (results not shown). Therefore, it seems that all alterations in these biomarkers are specific to malignant cell transformation. Also NIH/3T3 cell lines were infected with inactive MuSV virus stock, inactivated by heating at 70°C for 2 h, as an additional control. As expected, there were no significant differences in fluorescence compared with the control cells in the previously discussed spectral biomarkers.

Supervised classification and grading of premalignant fluorescence changes

After the validation of the above biomarkers (fluorescence intensities of aromatic amino acid and NADH) we used them to categorize and classify the samples at different stages of malignancy utilizing linear discriminant approaches. All above-mentioned transformations (40 of NIH/3T3 cell lines and 28 of MEF primary cells) were utilized for training.

Grading cancer progression by discriminant classification function

Each case was characterized using an array of biomarkers, which were arranged as follows: $\begin{pmatrix} \textit{Fluorescence of aromatic acids} \\ \textit{Fluorescence of NADH} \end{pmatrix}$.

Then we used a DCF as a statistical tool, which enables discrimination between premalignant stages to be improved by representing an adequate quantitative follow-up of transformations versus time. DCF generates a classification score for each case of postinfection day that is a linear combination of a previously derived array of biomarkers with weight coefficients. It has the following equation:

$$S = c + w_1 \cdot x_1 + w_2 \cdot x_2 + \cdots + w_m \cdot x_m, \quad (3)$$

where w_m is the weight coefficient, x_m is the biomarker value, c is a constant, and S denotes the resultant classification score. In such a representation there is freedom to define the weight coefficients and the constant c. In order to reduce score variability we adopted the following procedure: The weight coefficient of each biomarker was selected as follows: $w_i = (t_i/\text{average of normal value of tested biomarker})\cdot\alpha$, while the constants c and α were chosen in such a way as to nullify the average classification score of the normal group and give a score of 100 for completely transformed cells. t_i was defined as the paired t-value of each biomarker of malignant and control groups.

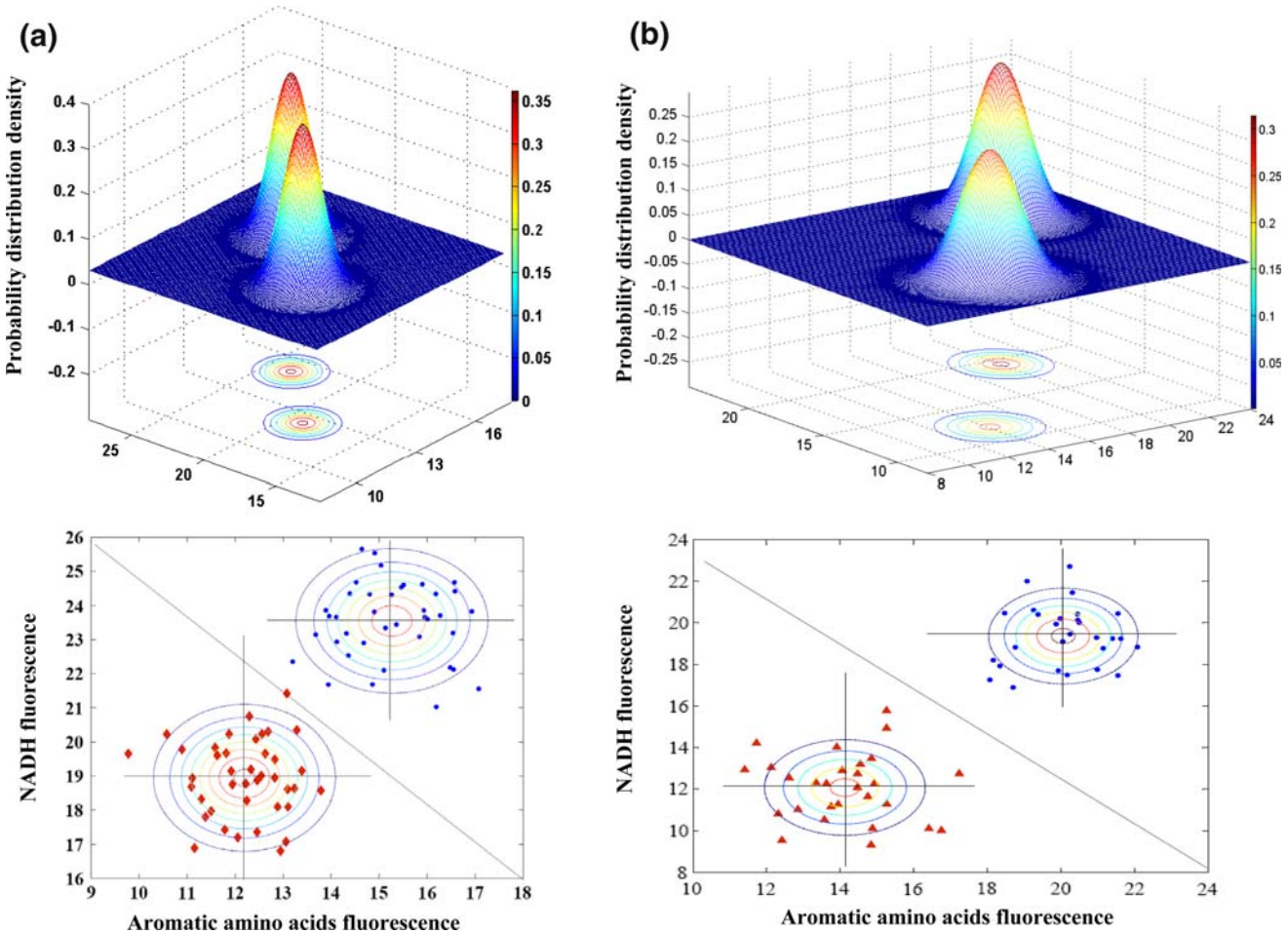

Fig. 3 Bivariate Gaussian model and Gaussian fit of trained data. The lower panels show the projections of the Gaussian distributions. **a** Normal murine fibroblast cell line (NIH/3T3) and completely transformed fibroblast cell line. **b** Normal mouse embryonic cells (MEF) and completely transformed mouse embryonic cells

According to the DCF (Fig. 4) there were no significant differences between the control cells and the postinfection cells at 2/4 h for both cells in culture (also assigned as 0-day infection group, morphologically similar to control cell cultures, as seen in Fig. 5a; there is also no growth on soft agar). Then we empirically divided the postinfection days of transformations into three premalignant stages. The first premalignant stage is a postinfection day when spectral discrimination between control and infected cells is possible, i.e., the *t*-values based on the discriminant classification score are significantly different between infected and control groups. In this stage it was still impossible to distinguish morphologically between these two types of cells. The second premalignant stage is an intermediate stage, which is significantly different from the first premalignant stage according to *t*-value based on the discriminant classification score; however, the first and second stage still morphologically resemble the control group. The last (third) stage is the postinfection day where the first morphological signs of malignancy become apparent (loss of contact inhibition and sharp edges of the cells; sharp edges and growing randomly in criss-cross fashion, as shown in Fig. 5b). This stage was also confirmed by examining the ability of the cells to grow on soft agar.

We observed fluorescence decreases versus postinfection time during the transformations of both cell cultures. The progression of transformations can be described by applying sigmoid fit (Fig. 4)

Supervised classification using LDA Mahalanobis distance

There are many possible techniques for classification of multivariate data. Principle component analysis (PCA) and LDA are two commonly used techniques for data classification and dimensionality reduction. LDA easily handles the case where the within-class frequencies are unequal.

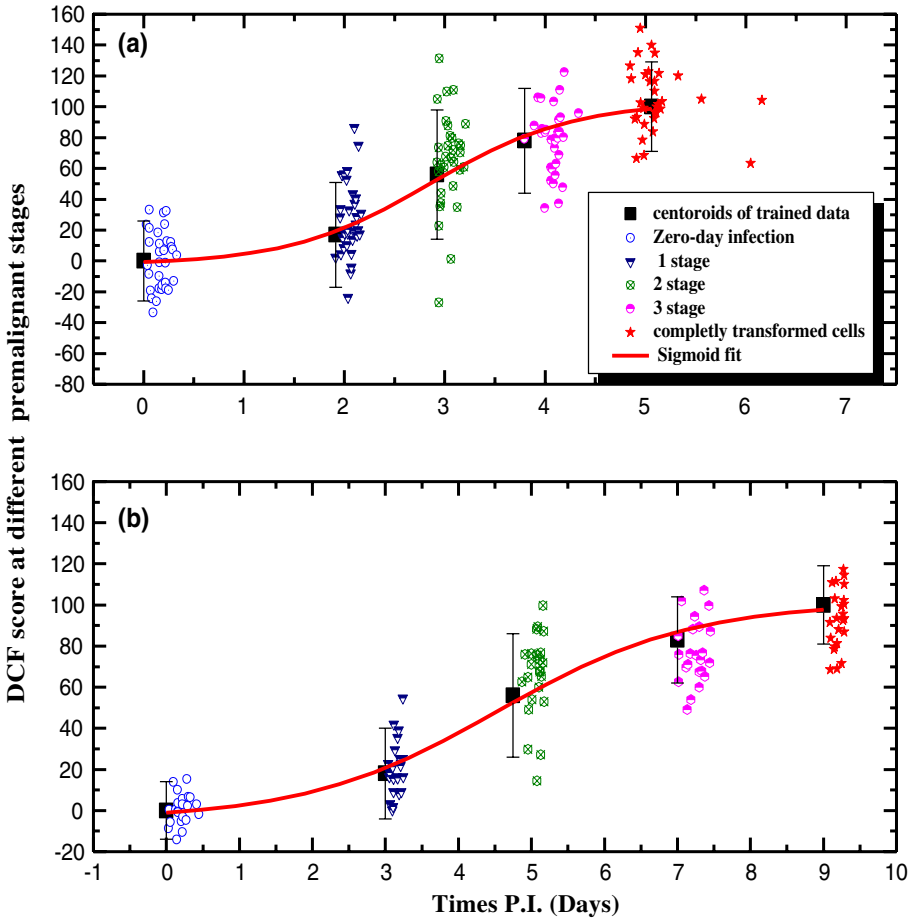

Fig. 4 Discriminant classification function. **a** NIH/3T3 cell line cancer progression. **b** MEF cell line cancer progression. Each case is a linear combination of two biomarkers from tested sample, while the sigmoid fit and the standard deviation were obtained from the average of training samples (*black squares*)

This method also maximizes the ratio of between-class variance to the within-class variance in any particular data set, thereby guaranteeing maximal separability (Fisher 1936; Huberty 1994; Fukunaga 1990). We decided to implement an LDA algorithm in order to provide better classification compared with PCA or classification based on Euclidean distance. Moreover, our results are represented as bivariate data; therefore, there is no necessity for dimensional reduction such as PCA or to design complex overfitting nonlinear structures such as neural networks.

In order to perform supervised classification we used previous 40 transformations of NIH/3T3 cell lines and 28 transformations of MEF cells to train our data set (i.e., obtain average vectors and covariance matrix for each of the five stages). After the parameters from training data were obtained, we assigned the item x from the tested cases to one of these five stages based on the closest Mahalanobis distance to the mean, which is expressed as follows:

$$d_j(x) = \sqrt{(x - \bar{x}_j)^T S_{\text{pl}}^{-1} (x - \bar{x}_j)}, \quad (4)$$

where $d(x)$ is the Mahalanobis distance of the item and S_{pl} is the pooled covariance matrix of multigroup.

We tested additional 32 transformations of NIH/3T3 cell lines and 22 transformations of MEF cells evaluating the potential of LIF for identification premalignant changes. Figure 4 shows the DCF score of these transformations.

The accuracy of identification premalignant stages varied from 85.6 to 96.4% for MEF primary cells and from 83.1 to 93.8% for NIH/3T3 cell lines (Table 1). The higher distinction observed in MEF cell cultures is related to their biological properties (as discussed later).

Discussion

In the present study we examined the potential of LIF to detect and distinguish premalignant changes of cell cultures due to viral cancerous transformation utilizing LDA approaches. The obtained results revealed that endogenous cellular fluorophores intensities consistently decreased during malignancy progression (Fig. 3). Even though there is a certain level of ambiguity to the biological interpretations, the gradual decline of aromatic amino acids and NADH coenzyme fluorescence due to carcinogenesis can arise from several cellular activities.

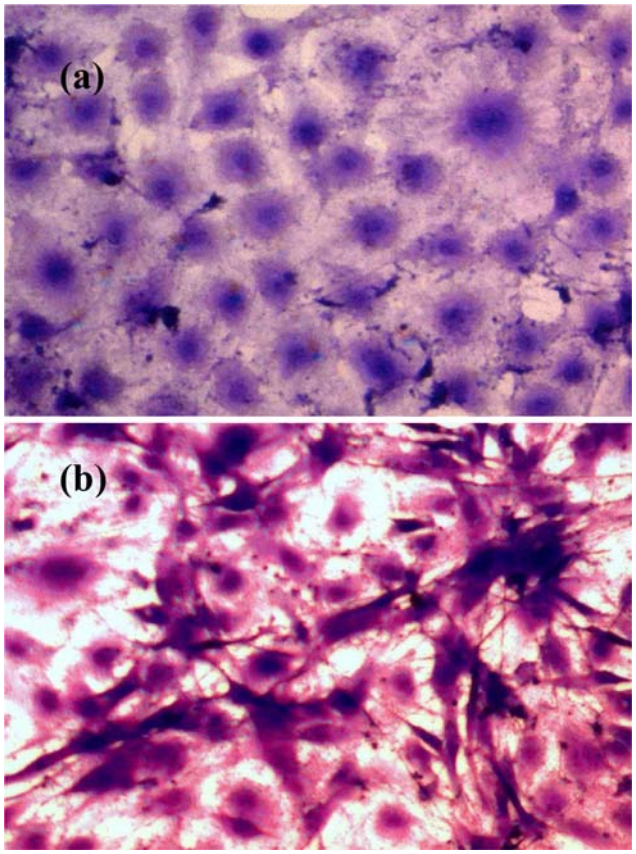

Fig. 5 Photomicrograph of cell cultures observed by light microscope with 40× magnification. **a** Control uninfected NIH/3T3 cell line. **b** Completely transformed NIH/3T3 cell line (NIH/3T3-MuSV)

Aromatic amino acids

The decrease in aromatic amino acids fluorescence intensities can be explained based on the enlargement of the cellular or/and the nuclear volume due to malignancy (Fig. 6, Drezek et al. 2003). Such alterations might certainly lead to higher light scattering in malignant cell cultures compared with control (Mourant et al. 2000), for example, Rayleigh scattering, which arises from small size regimes $x \ll 1$, where $x = \frac{2\pi r}{\lambda}$ (r is the characteristics dimension; in our case r is the size of aromatic amino acid, which is less than 1 nm, while λ is about 300 nm). Thus, elastic Rayleigh scattering will be involved in our cell cultures. The intensity of Rayleigh scattering for the single particle is defined as follows:

$$I = I_0 \frac{\pi^4 d^6}{8\lambda^4 R^2}(1 + \cos^2\theta)\left(\frac{n^2 - 1}{n^2 + 2}\right)^2, \quad (5)$$

where R is the distance to the particle, θ is the scattering angle, n is the refractive index of the particle, and d is the diameter of the particle. As a result of nuclei/cell enlargement (Fig. 6) increased scattering occurs with the light angular distribution ($1 + \cos^2(\theta)$), which eventually lead to decreased fluorescence efficiency in the malignant cells cultures relative to controls.

Another factor is related to the biochemical changes in proteins due to carcinogenesis. Tryptophan (the aromatic amino acid with highest quantum yield, i.e., a major contributor to fluorescence) is considered as very sensitive to its local environment (Lakowicz 1999; Valeur 2002), therefore changes in emission spectra may arise from conformational alterations, subunit association, substrate binding, denaturation, and anything that affects the local environment surrounding the indole ring. In addition, tryptophan appears to be uniquely sensitive to collisional quenching, either by externally added quenchers or by nearby groups in the protein (Lakowicz 1999; Valeur 2002; Mycek and Pogue 2003). In previous studies same

Table 1 Supervised classification of samples at different stages of malignant progression using LDA Mahalanobis distance

Cell cultures	Postinfection time	Stage	Accuracy* in %	False negative** in %	Number of samples	
					Tested	Trained
NIH/3T3	2 h	Zero-day infection	93.8	28	32	40
	2 days	Stage I	87.5	45.5		
	3 days	Stage II	83.1	68.4		
	4 days	Stage III	89.4	39.1		
	5 days	Malignant	95	33.3		
MEF	4 h	Zero-day infection	96.4	10	22	28
	3 days	Stage I	92.7	22.2		
	5 days	Stage II	87.3	46.7		
	7 days	Stage III	85.6	29.4		
	9 days	Malignant	92.7	22.2		

$* \text{Accuracy} = \frac{\text{true positive and true negative}}{\text{Total number of cases}} \cdot 100\%$

$** \text{ False negative rate} = \frac{\text{number of false negatives at each stage}}{\text{number of positive instance at each stage}} \cdot 100\%$

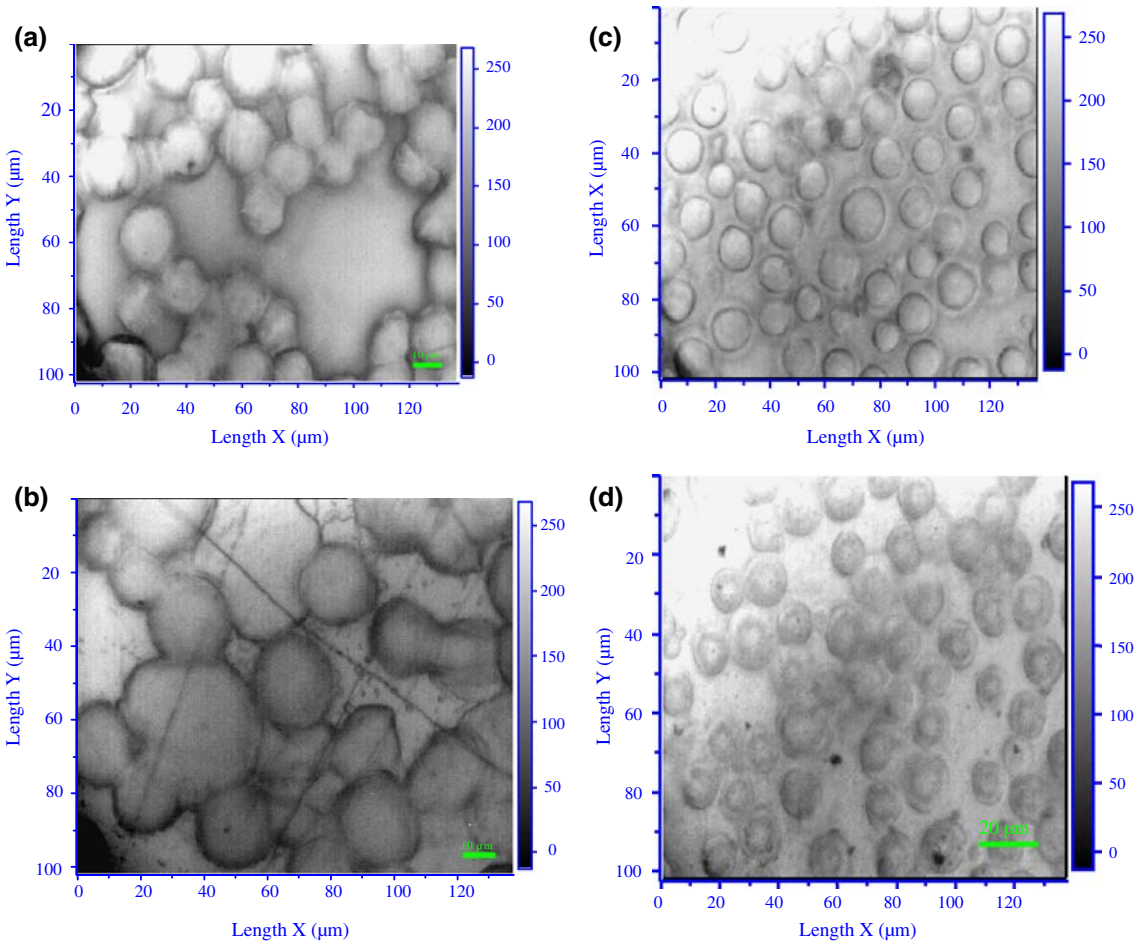

Fig. 6 Photomicrographs with 1,000× magnification of **a** control murine fibroblast cell line (NIH/3T3), **b** completely transformed fibroblast cell line (NIH/3T3-MuSV), **c** control mouse embryonic cells (MEF cells), and (**d**) completely transformed mouse embryonic cells (MEF-MuSV)

tendency of significant decrease in tryptophan fluorescence was reported in malignant human breast cell lines (Palmer et al. 2003) and stratified epithelium of cervical tissues (Martin et al. 2007). Decreased fluorescence was also found in tumorigenic murine fibroblasts cell cultures Balb/c3T3, transfected by H-ras under various physiological conditions (Grossman et al. 2001).

NADH

The diminishing of the reduced nicotinamide adenine dinucleotide (NADH) fluorescence in cell cultures can be interpreted using similar arguments to the decreasing aromatic amino acids fluorescence, i.e., variation in cellular and/or nuclear volumes.

The NADH coenzyme is an intrinsically fluorescent molecule that participates in oxidative energy metabolism. In the process of adenosine triphosphate (ATP) production, NADH molecule donates two electrons and becomes oxidized to NAD^+, which in contrast to NADH is not fluorescent. A sharp decrease of NADH/NAD^+ ratio may reflect high metabolic activity and cellular energy production due to malignancy. Reduced NADH fluorescence due to carcinogenesis was also reported in malignant sites of oral cavity tissues (Uppal and Gupta 2003). Another conformation of decreasing NADH/NAD^+ ratio in malignant cells was reported previously by Torabi et al. (1999). In this study, based on electrochemical measurements of NAD^+ and NADH concentrations in normal and cancer tissues, it was concluded that the NADH concentration is lower while the NAD^+ concentration is higher in cancer tissues compared with normal.

The initiation and progression of cancer can be characterized by sigmoid fits using spectral biomarkers array (Fig. 4). Similar behavior of malignant progression in these cells in culture have been obtained using Fourier-transform infrared (FTIR) microspectroscopy; for instance, there were observable spectral changes in the same period of time in protein vibrational modes (i.e., molecules resembling those involved in the present study), such as at 2,958 cm^{-1} (due to antisymmetric stretching of methyl groups) and at 1,171 cm^{-1} (mainly contributed by C–OH

groups of serine, threonine, and tyrosine amino acids) (Bogomolny et al. 2007, 2008).

According to the sigmoid fit we empirically divided the progression of premalignant stages as shown in Fig. 4. In a short interval of postinfection time, meaningfully shorter than the cell cycle, there are no detectable spectral differences between infected and control cell cultures. Then during a short time post infection (p.i.), infected cells reached stage 1 (2 days for NIH/3T3, 3 days for MEF), which offers significant spectral discrimination between normal and infected cells. This stage is still impossible to define by morphological means. In stage 2 the spectral difference becomes more evident. Then the spectral values of the infected cell cultures gradually approach the spectral values of the fully transformed cells and reach the third stage. In this period of postinfection time we can distinguish the first morphological signs. When cells in culture completely transformed to malignant, the fluorescence of biomarkers stabilized and clear malignant morphology appeared.

In the case of MEF transformation there is clear segregation between the premalignant stages, with the highest assessment of prognostic parameters (such as accuracy and false-negative rate, Table 1), which originates from the biological properties of these cells. Primary cells are completely different from the NIH/3T3 cell line in most of their characteristics (cell lines exist for a long time in culture while primary cells grow only for short periods of time in culture). MEF cells replicate slowly and are very sensitive to external factors. In fact, primary cells are very similar to normal organism cells in most of their characteristics, while cell lines are similar to malignant cells in some of their characteristics, such as fast replication and resistance to serum starvation.

The capability of LIF to detect early spectral biochemical changes due to malignant cell transformation compared with conventional methods such as morphological observation has tremendous advantage for the diagnosis of premalignant stages; for instance, diagnosis using Pap smear test has a very high rate of false negative (Solomon 2003), due to difficulty in detecting cells that are destined to become malignant but do not yet have clear apparent morphological characteristics.

Our results show that LIF and LDA approaches can classify and continuously grade premalignant stages with relatively high accuracy and low false-negative rate.

The use of cell culture may be considered a solid basis for evaluating the early detection potential of cancer in real tissues by this technique. Unlike cell culture, real tissues are much more complicated, not homogenous, and composed of various types of cells and blood vesicles. Therefore, the obtained specific spectral signals might be significantly lower compared with those obtained from cell cultures, which will hinder detection. Focusing on specific biomarkers acquired in cell cultures will make it much easier and more reliable to analyze the results obtained from real tissues. Though there are still requirements for designed clinical trials, overcoming the complexity of real tissue such as inhomogeneity, variations in thickness and/or amount of cells, and also the necessity for sample purification, LIF in tandem with proper statistical tools may be a promising technique for early detection of malignant progression, which is essential in cancer diagnosis and treatment.

References

Alfano RR, Das BB, Cleary J, Prudente R, Celmer EJ (1991) UV reflectance spectroscopy probes DNA and protein changes in human breast tissues. Bull N Y Acad Med 67:143–150

Alvarez RD, Wright TC, Optical Detection Group (2007) Effective cervical neoplasia detection with a novel optical detection system: a randomized trial. Gynecol Oncol 104:281–289. doi:10.1016/j.ygyno.2006.08.056

Bigio IJ, Mourant JR (1997) Ultraviolet and visible spectroscopies for tissue diagnostics: fluorescence spectroscopy and elastic-scattering spectroscopy. Phys Med Biol 42:803–814. doi:10.1088/0031-9155/42/5/005

Bogomolny E, Huleihel M, Suproun Y, Ranjit SK, Mordechai S (2007) Early spectral changes of cellular malignant transformation using Fourier transform infrared microspectroscopy. J Biomed Opt 12:024003–024008. doi:10.1117/1.2717186

Bogomolny E, Argov S, Mordechai S, Huleihel M (2008) Monitoring of viral cancer progression using FTIR–microscopy: a comparative study of intact cells and tissues. Biochim Biophys Acta 1780:1038–1046

Brancaleon L, Durkin AJ, Tu JH, Menaker G, Fallon JD, Kollias Nikiforos (2007) In vivo fluorescence spectroscopy of nonmelanoma skin cancer. Photochem Photobiol 73:178–183. doi:10.1562/0031-8655(2001)073<0178:IVFSON>2.0.CO;2

Breslin TM, Xu F, Palmer GM, Zhu C, Gilchrist KW, Ramanujam N (2004) Autofluorescence and diffuse reflectance properties of malignant and benign breast tissues. Ann Surg Oncol 11:65–70. doi:10.1007/BF02524348

Chaudhury NK, Chandra S, Mathew TL (2001) Oncologic applications of biophotonics. Appl Biochem Biotechnol 96:186–204. doi:10.1385/ABAB:96:1-3:183

Chidananda SM, Satyamoorthy K, Rai L, Manjunath AP, Kartha VB (2006) Optical diagnosis of cervical cancer by fluorescence spectroscopy technique. Int J Cancer 119:139–145. doi:10.1002/ijc.21825

Drezek R, Guillaud M, Collier T, Boiko I, Malpica A, Macaulay C, Follen M, Richards-Kortum R (2003) Light scattering from cervical cells throughout neoplastic progression: influence of nuclear morphology, DNA content, and chromatin texture. J Biomed Opt 8:7–16. doi:10.1117/1.1528950

Ebihara A, Krasieva T, Liaw LL, Fago S, Messadi D, Osann K, Wilder-Smith P (2003) Detection and diagnosis of oral cancer by light-induced fluorescence. Lasers Surg Med 32:17–24. doi:10.1002/lsm.10137

Fisher RA (1936) The use of multiple measures in taxonomic problems. Ann Eugen 7:179–188

Fukunaga K (1990) Introduction to statistical pattern recognition. Academic Press, San Diego

Georgakoudi I, Sheets E, Müller M, Backman V, Crum CP, Badizadegan K, Ramachandra D, Feld M (2002) Trimodal spectroscopy for the detection and characterization of cervical precancers in vivo. Am J Obstet Gynecol 186:374–382. doi:10.1067/mob.2002.121075

Grossman N, Ilovitz E, Chaims O, Salman A, Jagannathan R, Mark S, Cohen B, Gopas J, Mordechai S (2001) Fluorescence spectroscopy for detection of malignancy: H-ras overexpressing fibroblasts as a model. J Biochem Biophys Methods 50:53–56. doi:10.1016/S0165-022X(01)00175-0

Horak L, Zavadil J, Duchac V, Javorsky S, Kostkab F, Svec A, Lezal D (2006) Auto-fluorescence spectroscopy of colorectal carcinoma: ex vivo study. J Opt Adv Mater 8:396–399

Huberty C (1994) Applied discriminant analysis. John Wiley, New York

Kamath SD, Mahato KK (2007) Optical pathology using oral tissue fluorescence spectra: classification by principal component analysis and *k*-means nearest neighbor analysis. J Biomed Opt 12:014028. doi:10.1117/1.2437738

Krishna CM, Sockalingum GD, Vidyasagar MS, Manfait M, Fernanades DJ, Vadhiraja BM, Maheedhar K (2008) An overview on applications of optical spectroscopy in cervical cancers. J Cancer Res Ther 4:26–36. doi:10.4103/0973-1482.39602

Lakowicz JR (1999) Principles of fluorescence spectroscopy. Plenum Press, New York

Martin SF, Wood AD, McRobbie MM, Mazilu M, McDonald MP, Samuel ID, Herrington CS (2007) Fluorescence spectroscopy of an in vitro model of human cervical precancer identifies neoplastic phenotype. Int J Cancer 120:1964–1970. doi:10.1002/ijc.22517

Mayinger B, Horner P, Jordan M, Gerlach C, Horbach T, Hohenberger W, Hahn EG (2001) Light-induced autofluorescence spectroscopy for the endoscopic detection of esophageal cancer. Gastrointest Endosc 54:195–201

Mourant JR, Canpolat M, Brocker C, Esponda-Ramos O, Johnson TM, Matanock A, Stetter K, Frever JP (2000) Light scattering from cells: the contribution of the nucleus and the effects of proliferative status. J Biomed Opt 5:131–137. doi:10.1117/1.429979

Mycek M, Pogue BW (2003) Handbook of Biomedical Fluorescence. CRC Press, Boca Raton

Palmer GM, Keely PJ, Breslin TM, Ramanujam N (2003) Autofluorescence spectroscopy of normal and malignant human breast cell lines. Photochem Photobiol 78(5):462–469

Salman A, Ramesh J, Erukhimovitch V, Talyshinsky M, Mordechai S, Huleihel M (2003) FTIR microspectroscopy of malignant fibroblasts transformed by mouse sarcoma virus. J Biochem Biophys Methods 55:141–153. doi:10.1016/S0165-022X(02)00182-3

Sokolov K, Follen M, Richards-Kortum R (2002) Optical spectroscopy for detection of neoplasia. Chem Biol 6:651–658

Solomon D (2003) Screening for cervical cancer: prospects for the future. J Natl Cancer Inst 85:1018–1019. doi:10.1093/jnci/85.13.1018

Svanberg K, Wang I, Colleen S, Idvall I, Ingvar C, Rydell R, Jocham D, Diddens H, Bown S, Gregory G, Montán S, Andersson-Engels S, Svanberg S (1998) Clinical multi-colour fluorescence imaging of malignant tumours—initial experience. Acta Radiol 39:2–9

Torabi F, Ramanathan K, Larsson PO, Gorton L, Svanberg K, Okamoto Y, Danielsson B, Khayyami Y (1999) Coulometric determination of NAD^+ and NADH in normal and cancer cells using LDH, RVC and a polymer mediator. Talanta 50:787–797. doi:10.1016/S0039-9140(99)00134-4

Uppal A, Gupta PK (2003) Measurement of NADH concentration in normal and malignant human tissues from breast and oral cavity. Biotechnol Appl Biochem 37:45–50. doi:10.1042/BA20020052

Valeur B (2002) Molecular spectroscopy. Principles and applications. Wiley, Weinheim

Wang H, Willis J, Canto M, Sivak MV, Izatt JA (1999) Quantitative laser scanning confocal autofluorescence microscopy of normal, premalignant, and malignant colonic tissues. Trans Biomed Eng 46:1–7. doi:10.1109/TBME.1999.804578

Zheng W, Olivo M, Soo KC (2004) The use of digitized endoscopic imaging of 5-ala-induced ppix fluorescence to detect and diagnose oral premalignant and malignant lesions in vivo. Int J Cancer 110:295–300. doi:10.1002/ijc.20080